ADVANCES IN ATMOSPHERIC SCIENCES, VOL. 27, NO. 3, 2010, 562–574

Aerosol Optical Properties Affected by a Strong Dust Storm over Central and Northern China

XIN Jinyuan[1] (辛金元), DU Wupeng*[1,2] (杜吴鹏), WANG Yuesi[1] (王跃思), GAO Qingxian[3] (高庆先), Zhanqing LI[4], and WANG Mingxing[1] (王明星)

[1] *State Key Laboratory of Atmospheric Boundary Layer Physics and Atmospheric Chemistry, Institute of Atmospheric Physics, Chinese Academy of Sciences, Beijing* 100029

[2] *Beijing Climate Center, Beijing Meteorological Bureau, Beijing* 100089

[3] *Chinese Research Academy of Environment Science, Beijing* 100012

[4] *Department of Meteorology, the University of Maryland, College Park, MD* 20782, *US*

(Received 26 February 2009; revised 26 July 2009)

ABSTRACT

Aerosol observational data at 8 ground-based observation sites in the Chinese Sun Hazemeter Network (CSHNET) were analyzed to characterize the optical properties of aerosol particles during the strong dust storm of 16–21 April 2005. The observational aerosol optical depth (AOD) increased significantly during this dust storm at sites in Beijing city (86%), Beijing forest (84%), Xianghe (13%), Shapotou (27%), Shenyang (47%), Shanghai (23%), and Jiaozhou Bay (24%). The API (air pollution index) in Beijing and Tianjin also had a similar rise during the dust storm, while the Angström exponent (α) declined evidently at sites in Beijing city (21%), Beijing forest (39%), Xianghe (19%), Ordos (77%), Shapotou (50%), Shanghai (12%), and Jiaozhou Bay (21%), respectively. Furthermore, The observational AOD and α demonstrated contrary trends during all storm stages (pre-dust storm, dust storm, and post-dust storm), with the AOD indicating an obvious "Valley–Peak–Valley" pattern of variation, while α demonstrated a "Peak–Valley– Peak" pattern. In addition, the dust module in a regional climate model (RegCM3) simulated the dust storm occurrence and track accurately and RegCM3 was able to basically simulate the trends in AOD. The simulation results for the North China stations were the best, and the simulation for dust-source stations was on the high side, while the simulation was on the low side for coastal sites.

Key words: optical properties, dust storm, RegCM3, aerosol optical depth (AOD), Angström exponent (α)

Citation: Xin, J. Y., W. P. Du, Y. S. Wang, Q. X. Gao, Z. Q. Li, and M. X. Wang, 2010: Aerosol optical properties affected by a strong dust storm over central and northern China. *Adv. Atmos. Sci.*, **27**(3), 562–574, doi: 10.1007/s00376-009-9023-5.

1. Introduction

In northern China, dust is an important component in atmospheric aerosols and dust storms occur quite frequently, which is due in large part to the arid land surface and large wind speed during spring. Wind-blown dust, and especially in dust storms, has a remarkable impact on the exchange of aerosol optical properties and can obviously increase the atmospheric dust particle burden (Zakey et al., 2006; Xin et al., 2007; Du et al., 2008). Northern China is the second largest source region for atmospheric dust aerosol in the world (Zhang et al., 1996; Chen et al., 2006), and annual dust and sand emissions in the area amount to over 25 million tons (Xuan et al., 2000). Furthermore, dust particles play an important role in troposphere atmosphere (Zhang et al., 2003a; Wang et al., 2007a, b). In many arid and semi-arid areas, such as northwestern China, sand-dust is one of the most important aerosol particles (Zhou et al., 2002; Zhang et al., 2003a; Li et al., 2005). To this end, it is necessary to understand the aerosol optical properties variations af-

*Corresponding author: DU Wupeng, duwupeng@sina.com

fected by strong dust storms over central and northern China.

Some researchers have indicated that strong dust storms with sources in China's deserts can arrive in North America across the Pacific via the high-altitude westerlies, and provide an important contribution to atmospheric aerosol loads, especially in the spring (Zhang, 2001; Song et al., 2004). Zhang found that 30% of the Chinese atmospheric desert dust is redeposited onto the deserts, 20% is transported over regional scales, and the remaining 50% of the dust is subjected to long-range transport to the Pacific Ocean and beyond (Zhang et al., 1997). Measurements also suggest that the sandy land in northeastern China is a potential source for Asian dust, and mass backtrajectory analysis showed that five major transport pathways of Asian dust storms dominated dust transport in China during spring 2001, all of which passed over Beijing (Zhang et al., 2003b). Long-distance transport of dust storms not only changes the atmospheric dynamic structure in dust source regions, but also exerts a certain extent on the downstream atmospheric structure and land-atmosphere radiation energy balance in Korea, Japan, North America, and the Pacific region; thereby dust storms can change the atmospheric circulation and have an important impact on the regional and global environment, and has implications for climate change, which currently garners considerable attention by governments and researchers (Seinfeld et al., 2004; Won et al., 2004; Zhang et al., 2004; Kim et al., 2006; Shao et al., 2007). At present, China's research on atmospheric aerosols, including dust aerosol, is focused on statistical analysis aimed at the short-medium periodic aerosol characteristics in a single regional, continental, or even global long-term aerosol climate effect simulation (Mao et al., 2002; Tian et al., 2005; Liu et al., 2008), whereas research activity utilizing regional observation networks or analyzing of aerosol properties changing significantly due to short-term weather, such as a strong dust storms, is less.

Ground-based network observations (Holben et al., 2001; Ogunjobi et al., 2007; Qiu et al., 2007; Xin et al., 2007; Du et al., 2008; Liu et al., 2008; Wang et al., 2008) and model simulation (Tegen and Fung, 1994; Gong et al., 2003; Chen et al., 2006; Zakey et al., 2006) are the key methods for research of regional aerosol optical properties. Ground-based network observations have the advantage of higher precision and better time resolution, and can provide the most effective and useful verification data for simulation, but there are temporal and regional limitations (Holben et al., 2001; Kim et al., 2004; Kolev et al., 2007). Numerical simulation is an important tool for detailed understanding of dust storm occurrence, transport, trajectory, and dust aerosol optical properties and radiation characteristics (Chen et al., 2006; Solmon et al., 2006; Zakey et al., 2006; Du et al., 2008). Han used a Regional Air Quality Model (RAQM) to simulate Asian dust storms, and the validation demonstrated a good capacity of the model system to capture most of the key features of dust evolution while reproducing the particle mass size distribution along the transport pathway of soil dust (Han et al., 2004). Wu compared two surface-dust emission schemes in the regional climate model RegCM3 in East Asia, showing that obvious differences exist in dust emission quantity and its column burden, and there were some uncertainties in simulating mineral dust aerosol by modeling (Wu et al., 2006). The aerosol concentration and optical depth obtained from dust models can make up for a lack of data from ground-based observational networks and satellite inversions of aerosol vertical structure properties and spatiotemporal distribution, and is more suitable for judgments of global or regional aerosol characteristics (Zakey et al., 2006; Du et al., 2008). To this end, the associated use of a ground-based observation network and numerical modeling has an important scientific basis for the detailed quantitative research of atmospheric aerosol optical properties in dust storm conditions (Zakey et al., 2006; Du et al., 2008).

Given these remarks, research on dust aerosol optical properties has an important scientific significance, and in this paper, we discuss a typical dust storm's effects on northern China's aerosol optical depth and wavelength index (α), and we also analyze this dust storm's weather processes from backward trajectories to the observational sites in detail. As an important supplement, we also provide simulation results for changes in dust AOD characteristics and compare the observed AOD with simulation by a regional climate model during this dust storm.

2. Principle and method

At first, this study used the Chinese Sun Hazemeter Network (CSHNET) observational results, such as aerosol optical depth (AOD) and wavelength index (α), to analyze the effect of a particular dust storm (16–21 April 2005) on aerosol optical properties in China's northern region, and the air pollution index (API) of Beijing and Tianjin was also used to indicate the dust storm's effect on the atmospheric environment. Then, we employed the Meteorological Information Comprehensive Analysis and Process System (Micaps) and a backward trajectory method to analyze and track this dust storm process preliminarily. Finally, the third-generation Regional Climate Model (RegCM3) was used to simulate the dust storm occur-

rence and trajectory, and the ground-based observation data were used to verify the simulation results.

2.1 *Aerosol observation network and data description*

The Institute of Atmospheric Physics (IAP), the Chinese Academy of Sciences (CAS), and the University of Maryland developed the Chinese Sun Hazemeter Network (CSHNET) in July 2004. As China's first and largest set of ground-based aerosol observation platforms, the observation sites can provide important data for researching regional aerosol optical properties and their subsequent climatic and environmental effects (Xin et al., 2006, 2007; Du et al., 2008). LED (Light-emitting Diode) hazemeters, which have been widely employed in the GLOBE (Global Learning and Observations to Benefit the Environment) program and are generally recognized by international scientists (Brooks and Mims, 2001; Hao et al., 2005; Acharya, 2005), were uniformly used for all observation sites. The measurement period lasted from 10 am to 2 pm (local standard time), with a measurement frequency of once per ten minutes. Weather conditions and cloud cover were synchronously recorded during the measurement period. The instrument has four wavelength channels (880 nm, 650 nm, 500 nm, and 405 nm) for the sunphotometer, and here the 500 nm channel is used for discussing the AOD and α reported in this paper.

Due to the occurrence and obvious influence of spring dust storms, primarily in northern China, we selected 8 sites in the ground-based observation network for good regional representation, including: Beijing city, Beijing forest (Beijing Dongling mountain forest), Xianghe, Ordos, Shapotou, Shenyang, Shanghai city, and Jiaozhou Bay (Fig. 1).

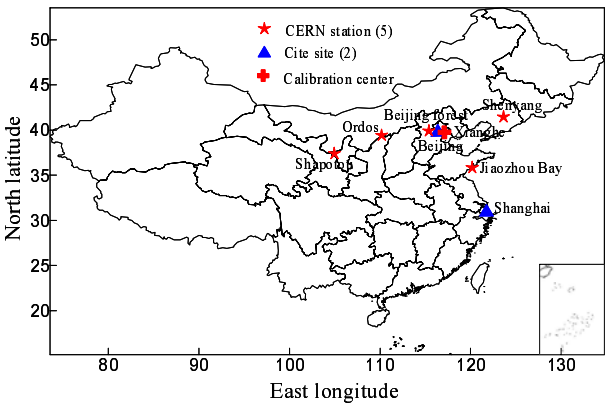

Fig. 1. Distribution of observation sites in the Chinese Sun Hazemeter Network (CSHNET). The sites include CERN (Chinese Ecosystem Research Network) sites, city sites, and a calibration center (Xianghe station).

2.2 *Model introduction and simulation design*

RegCM3 can not only simulate the climate features and trends on the regional scale, but also has good simulation capability for weather events (Zakey et al., 2006; Elguindi et al., 2007). Currently, most research and applications using RegCM3 are regional climate simulations, such as the simulation and verification of inter-decadal average temperature, precipitation, and other meteorological factors (Gao et al., 2003; Shi and Wang, 2003), but it is rare to use RegCM3 to simulate and verify short period weather changes, such as a dust storm. RegCM3 has been widely applied in regional climate research because of better resolution and more detailed physical processes (Qian et al., 1999; Elguindi et al., 2007) than global models. The model simulation is easy to control and is predictable, but the model mechanism is complex, and the criterion of results verification is strict and rigorous (Solmon et al., 2006; Elguindi et al., 2007).

In RegCM3, the dust emission calculation is based on parameterization of soil aggregate saltation and sandblasting processes. The main steps in the calculation include the specification of the soil aggregate size distribution for each model grid cell, the calculation of a threshold friction velocity leading to the erosion and saltation processes, the calculation of horizontal saltating soil aggregate mass flux, and finally the calculation of vertical transportable dust particle mass flux generated by saltating aggregates (Zakey et al., 2006; Elguindi et al., 2007).

The number of particle size bins effectively transported by the model has been set to four types to reduce computational costs, with sizes 0.01–1, 1–2.5, 2.5-5, and 5–20 μm, respectively. For each of the four bins, the corresponding emissions are calculated by aggregation of the defined emission sub-bins. Each transport bin is considered as a distinct tracer and is transported according to the tracer transport equation (Solmon et al., 2006). This includes transport by resolvable scale winds, sub-grid scale turbulence, and deep convection, along with wet and dry removal processes.

The wet deposition is treated following Giorgi for resolvable scale precipitation and Giorgi and Chameides for convective precipitation (Giorgi and Chameides, 1986; Giorgi, 1989; Solmon et al., 2006). The dry deposition velocities are calculated as a function of particle size and density and include the contributions of turbulent transfer, Brownian diffusion, impaction, interception, gravitational settling, and particle rebound (Giorgi and Chameides, 1986; Zhang, 2001).

Dust optical properties are computed for each size bin of the RegCM radiation scheme using a Mie scattering code, and a sub-bin size distribution is assumed

for these calculations following the approach described by Zender (Zender et al., 2003). In reality, dust optical parameters may vary depending on source region, composition, particle size, and many other parameters (Formenti et al., 2003; Haywood et al., 2003), but, this complexity is not accounted for in the present dust scheme configuration.

The simulation region mainly covers the Chinese mainland, and the map projection is Lambert; horizontal resolution is 60 km with a three-level nested grid for terrain, so the terrain resolution reaches 20 km at maximum. The central location is 36.5°N, 102°E; initial and boundary data is from NCEP (National Centers for Environmental Prediction) reanalysis data (2.5°× 2.5°, 17 levels) and NOAA (National Oceanic and Atmospheric Administration) weekly sea temperature data (1°×1°). Vegetation and terrain height data are obtained from USGS (United States Geological Survey). The detailed physical parameters schemes used are exponential relaxation at the lateral boundary, a Holtslag planetary boundary layer (Holtslag et al., 1990), the Grell convection scheme (Grell, 1993), the sub-grid explicit moisture scheme, the Zeng ocean flux parameterization scheme (Zeng et al., 1998), and chemical process and feedback mechanism are also considered in the simulation. In the simulation, 20 days of spin-up time is used.

In addition, the HYSPLIT-4 (HYbrid Single-Particle Lagrangian Integrated Trajectory) model system was also used in this paper, which was developed by National Oceanic and Atmospheric Administration (NOAA) and was used to analyze particle tracks, diffusion, and sedimentation (Draxler and Rolph, 2003; Rolph, 2003). This model belongs to the Eulerian-Lagrangian mixture diffusion family, and its calculation in the stratosphere and for diffusion adopts a Lagrangian format. HYSPLIT-4 is usually used to track the direction of movement for airflow or particles, and for real-time forecasts of wind field changes and analysis of atmospheric precipitation. HYSPLIT-4 employs a Sigma vertical coordinate with 28 levels and its horizontal grids are same as the meteorological fields, and the meteorological elements are linearly separated into the sigma layers, in this paper. NCEP FNL (Final) Operational Global Analysis data was used in the backward trajectory analysis.

3. Weather situation and backward trajectory analysis

3.1 *Observational weather situation*

The occurrence and trajectory of dust storms have a very close relation with meteorological conditions, and large numbers of dust particles can undergo long-distance transport to eastern China under the control of northwesterly airflow. The strong dust storm of 16–21 April in 2005 was one of the most extensive and serious sandstorms in recent years, and its region of influence included Inner Mongolia, Qinghai, Gansu, Ningxia, Shaanxi, Shanxi, Hebei, Beijing, Tianjin, Henan, Shandong, and 10 other provinces (municipalities and autonomous regions). Figure 2 shows the 850 hPa geopotential height field at 0800 LST, 16–21 April 2005, and according to the analysis and comparison of the geopotential height field and simulated dust storm process in section 5.1 in this paper, it is clear that a strong westerly wind moved toward the east and carried a large amount of dust particles with sources in Inner Mongolia, Gansu, Shaanxi, and Ningxia on 16 April. The main trough was located in Northwest China at this time and formed a certain scale of sandstorm; the leading edge of the trough and the dust storm affected parts of North and Northeast China and caused serious dust weather phenomenon on 17 April. We also can see from the geopotential height field figures that another strong trough appeared in Northwest China that brought heavy westerly winds, which carried plentiful sand-dust and moved from west to southeast on 18 April, and the strong wind arrived in North and Northeast China on 19 April, resulting in the re-emergence of serious dust weather in these regions. Dust storm weather began to significantly affect the Yangtze River basin and parts of East and South China after 19 April, and westerly front had weakened and moved out of China's mainland gradually after 21 April. Furthermore, the suspended dust aerosol in atmosphere began to decrease at the same time, and the dust particle concentration and dust AOD also declined gradually.

3.2 *Backward trajectory analyses*

We take the Beijing city site (39.97°N, 116.37°E), the Beijing forest site (39.97°N, 115.43°E), the Xianghe site (39.75°N, 116.96°E), the Ordos site (39.48°N, 110.18°E), the Shapotou site (37.45°N, 104.90°E), the Shenyang site (41.52°N, 123.63°E), the Shanghai site (31.12°N, 121.75°E), and the Jiaozhou Bay site (35.90°N, 120.18°E) as the reference centers, choosing 500 m as the height level, and use the HYSPLIT-4 model system to calculate the five-day backward trajectories for all observation sites on 21 April 2005, to track the past 120 hours of air mass routes (Fig. 3).

It can be seen from backward trajectories figures (Fig. 3) that during 16–21 April, the air masses in question which affected Beijing city, Beijing forest, and the Xianghe site were mainly from central and eastern Mongolia and central Inner Mongolia; the air masses affecting Ordos and Shapotou mainly came from

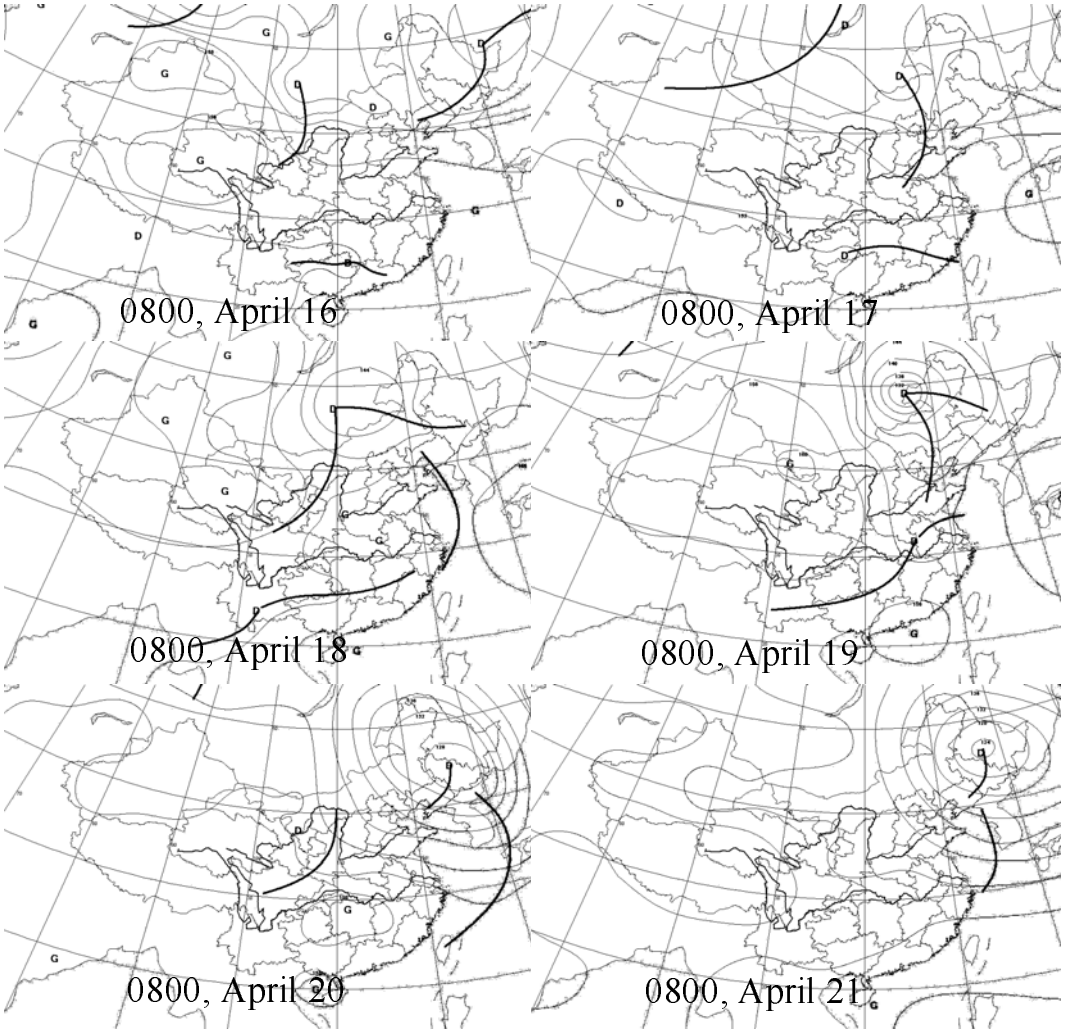

Fig. 2. East Asia 850 hPa geopotential height field at 0800 LST, 16–21 April 2005.

Mongolia and central and western Inner Mongolia, Gansu, Ningxia, and other China's northwestern regions; meanwhile, the Shenyang site was chiefly impacted by the local air mass sourced from Northeastern China and eastern Mongolia; furthermore, the Shanghai and Jiaozhou Bay sites were basically impacted by the air masses sourced from Mongolia, and central and western Inner Mongolia. We also can see from Fig. 3 that the movement of air masses was rapid, which indicated that the wind speed was relatively fast during the period of 16–21 April. This, coupled with the fact that spring precipitation is scarce and the land surface soil is loose in Mongolia and northwestern China, means that dust storms are easy form under the presence of strong wind. As a result, North, Northwest, Northeast, and East China were controlled by strong northwesterly airflow that carried large a number of dust particles, resulting in the emergence of obvious dust weather when air masses passed through the above regions on 16–21 April. In addition, the

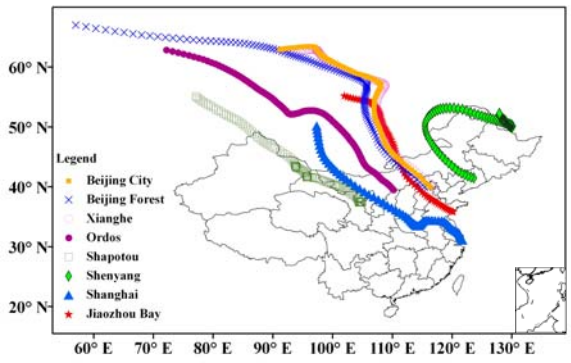

Fig. 3. The backward trajectories for the Beijing city, Beijing forest, Xianghe, Ordos, Shapotou, Shenyang, Shanghai, and Jiaozhou Bay. Height level is 500 m; track time is 120 hours; start time is 0800 LST 21 April 2005.

Table 1. Changes in AOD and comparison for different observation sites in different periods (500 nm).

	AOD changes at observation sites							
Periods	Beijing city	Beijing forest	Xianghe	Ordos	Shapotou	Shenyang	Shanghai	Jiaozhou Bay
Pre-dust storm	0.37	0.19	0.40	0.25	0.22	0.53	0.81	0.63
Dust storm	0.69	0.35	0.45	0.25	0.28	0.78	1.00	0.78
Post-dust storm	0.27	0.20	0.32	0.23	0.22	0.49	0.90	0.66

Table 2. Changes in α and comparison for different observation sites in different periods (500 nm).

	α changes at observation sites							
Periods	Beijing city	Beijing forest	Xianghe	Ordos	Shapotou	Shenyang	Shanghai	Jiaozhou Bay
Pre-dust storm	1.35	0.79	1.02	0.35	1.11	0.76	1.10	0.94
Dust storm	1.07	0.48	0.83	0.08	0.55	0.87	0.97	0.74
Post-dust storm	1.19	0.73	0.95	0.37	0.73	1.05	0.84	0.89

backward trajectories and 850 hPa geopotential height field (Fig. 2) are basically in agreement with each other after detailed comparison and analysis.

4. The influence of dust storm on aerosol optical properties

Photometer observations are not suitable for use in some special weather conditions (such as cloudy, during precipitation, etc.), so the observational data sometimes may be not continuous. Taking account of the dust storm trajectory direction (from west to east), different geographical locations for various observation sites, and the atmospheric environmental characteristics of "first pollution, second dust-sand" caused by the dust storm, we generally divide 12–25 April into three periods: pre-dust storm (12–15 April), dust storm (16–21 April), and post-dust storm (22–25 April), and we calculate and discuss the average AOD and wavelength index (α) for different sites in these three typical periods, respectively.

4.1 *The AOD and α characteristics observed by CSHNET*

Figure 4 shows the trends of aerosol optical depth (AOD) and wavelength index (α) at Beijing, Beijing forest, Xianghe, Ordos, Shapotou, Shenyang, Shanghai, and Jiaozhou Bay during 12–25 April 2005, respectively (AOD figures are on the left, α figures are on the right). It can be seen that observational AOD values presented "low–high–low" trends, basically. There was no sandstorm weather and the better air quality lasted for 3–4 days after 12 April, with the contribution and impact of dust aerosol particles relatively weak within the overall aerosol burden, and the aerosol optical depth lower during the pre-dust storm period (Fig. 4). The ground-based observational AODs were gradually elevated with the occurrence of the sandstorm and the increase of dust particles in atmosphere. Finally, in the post-dust storm period, the dust weather gradually weakened after it influenced China's mainland, and observational AODs began to reduce obviously accompanied with the end of this sandstorm (Fig. 4).

The wavelength index (α) was clearly showed an inverse pattern with the AOD trends (Fig. 4) and displayed "high-low-high" trends in the stages of pre-dust storm, dust storm, and post-dust storm, respectively. The average α value was higher before the occurrence of dust storm, and it demonstrated that the aerosol particle size was smaller, and the coarse-mode dust particle was a smaller part of the whole atmospheric aerosol load, and the affect of dust on the air quality was not obvious. With the occurrence of the sandstorm and the increase of the dust aerosol concentration, the observational α value decreased gradually to a certain degree. In contrast, the dust particle amount in the atmosphere was reduced greatly and the aerosol content decreased simultaneously with the end of this dust storm, and correspondingly the ground-based observational α values began to rise again gradually after this.

We can see clearly from Fig. 4, Table 1, and Table 2 that this dust storm had an obvious impact on atmospheric AOD and α. The AOD value was markedly high during 16–21 April, such that the average AOD increased to 0.69, 0.73, and 0.78 from 0.37, 0.53, and 0.63 at the Beijing city, Shenyang, and Jiaozhou Bay sites, respectively. The increases were 86%, 84%, 13%, 27%, 47%, 23%, and 24% at the Beijing city, Beijing forest, Xianghe, Shapotou, Shenyang, Shanghai, and Jiaozhou Bay sites, respectively. In contrast, the AOD declined gradually with the end of dust storm weather, with reductions from 0.35 to 0.20 at the Beijing forest

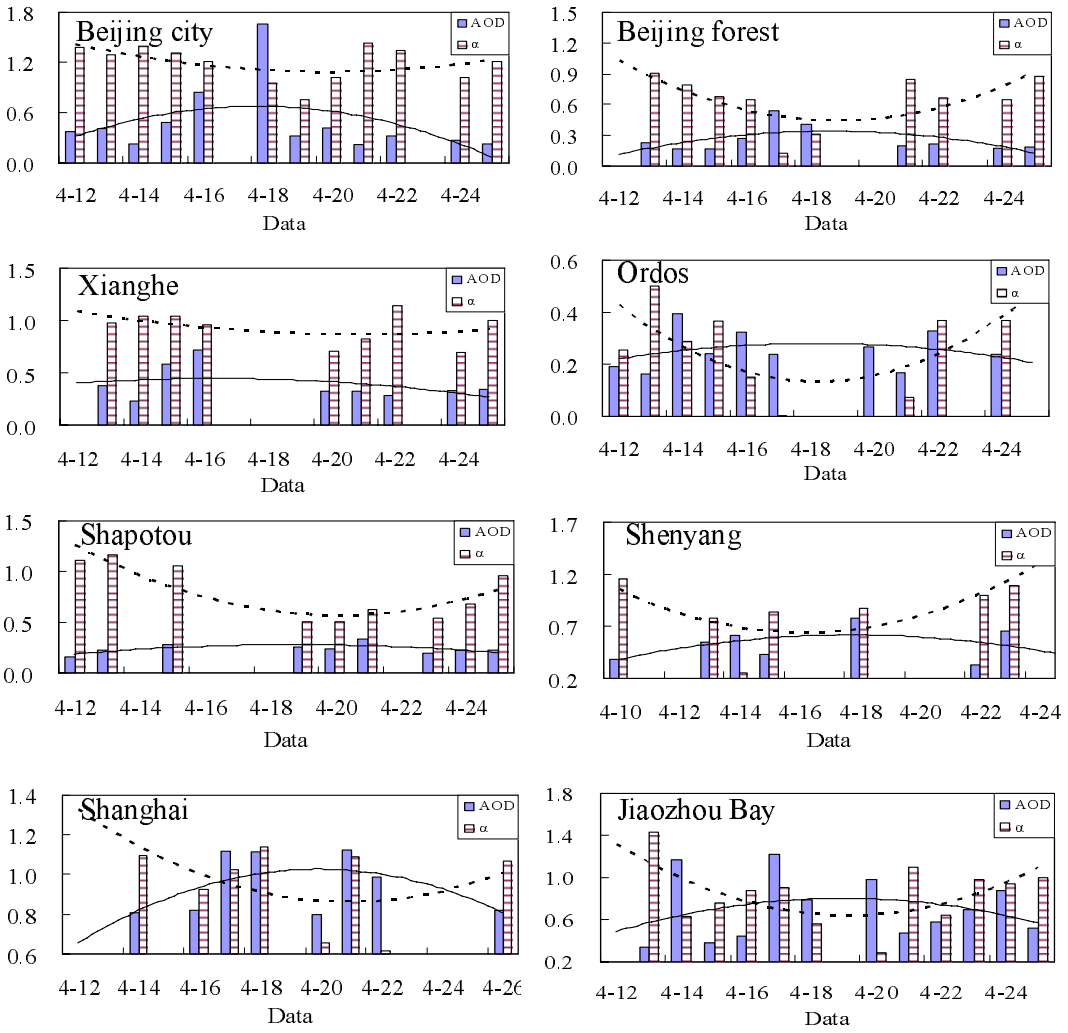

Fig. 4. Observational AOD and α trends during this dust storm at 500 nm in CSHNET.

site, from 0.45 to 0.32 at the Xianghe site, and from the 0.28 to 0.22 at the Shapotou site, respectively, equivaent to 57%, 71%, and 79% of their respective original AOD values. The aerosol wavelength index was the lowest during the period of the dust storm, with decr-

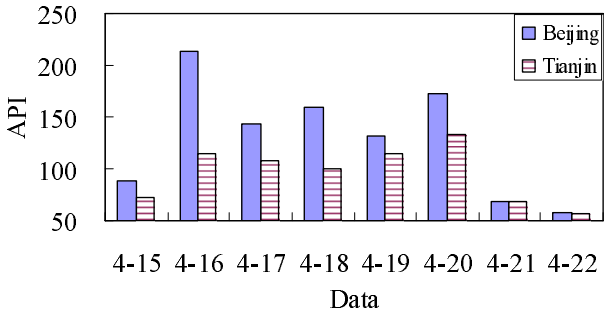

Fig. 5. The API during 15–22 April at Beijing and Tianjin.

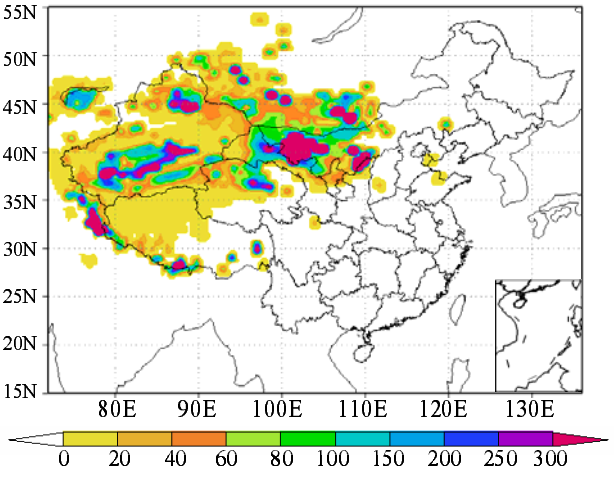

Fig. 6. Surface dust emission intensity in RegCM3 (μg m^{-2} s^{-1}).

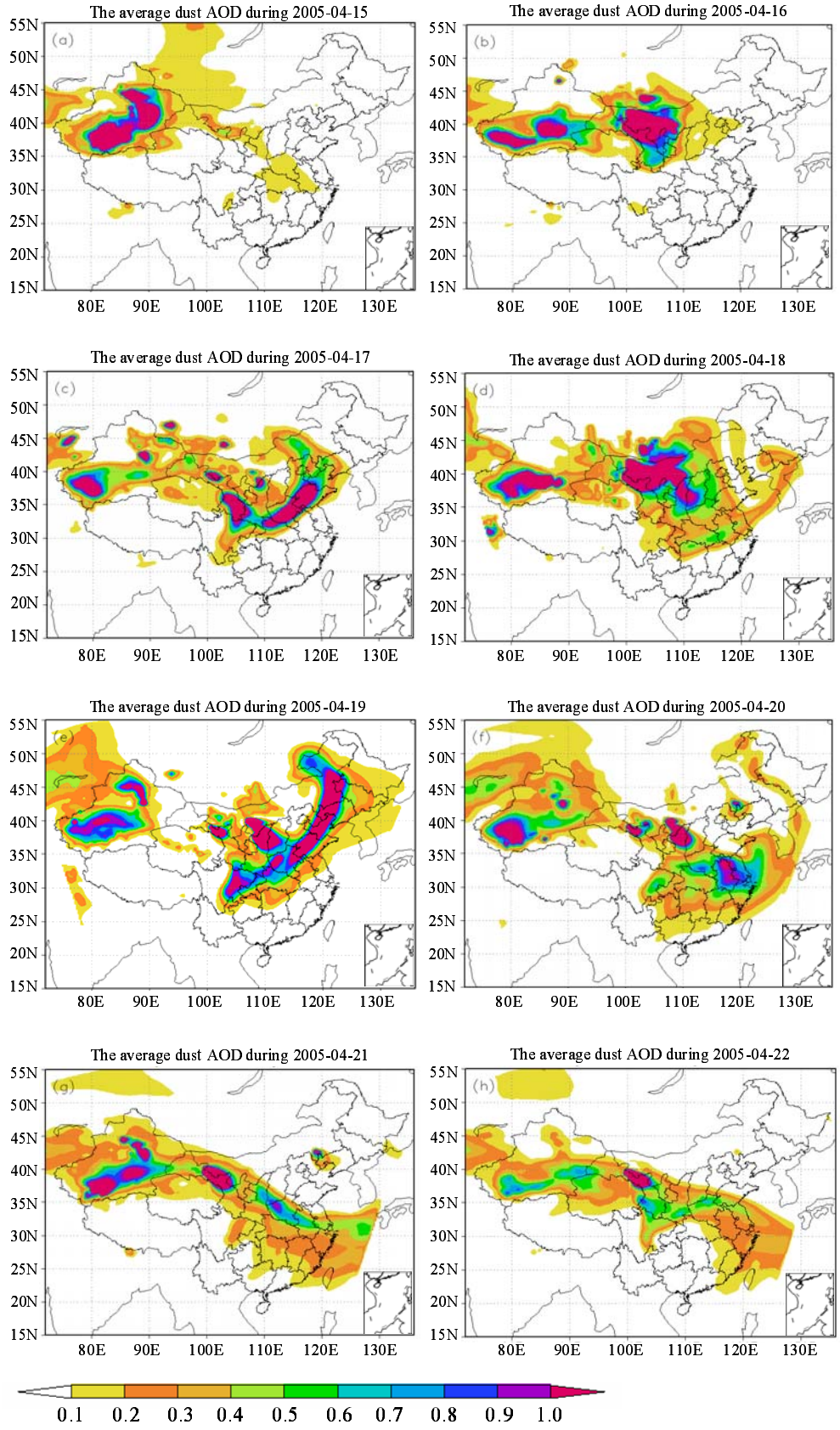

Fig. 7. The dust AOD variation during 15–22 April simulated by RegCM3 (1200 LST). The color scale applies to all panels.

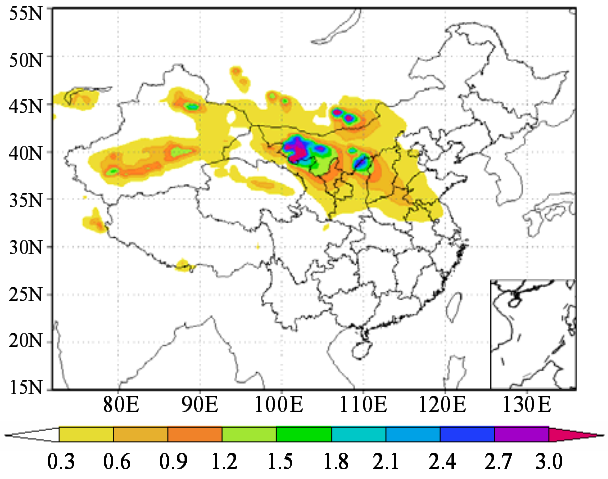

Fig. 8. The dust aerosol average column burden for 15–22 April simulated by the model (g m^{-2}).

eases of 21%, 39%, 19%, 77%, 50%, 12%, and 21% at the Beijing city, Beijing forest, Xianghe, Ordos, Shapotou, Shanghai, and Jiaozhou Bay sites, respectively. The average α was 1.35 for 12–15 April, while it declined to 1.07 and rose to 1.19 at Beijing city. During 12–15 April, the average α was 0.79 at the Beijing forest site; however, it was 0.48 for 15–21 April, and it was 0.73 for 22–25 April. It was similar at the Jiaozhou Bay site, where α was 0.94, 0.74, and 0.89 for 12–15, 16–21, and 22–25 April. It is worth noting that the date of the α decline was distinctly different at Shenyang site, perhaps because this site was closer to the dust source of Mongolia and central and eastern Inner Mongolia, and so the affected period by dust storm occurred earlier. On the other hand, the Shanghai site was far away from the dust source and it was late to be affected by the sandstorm, which led to observation that α was still relatively small on 22 April.

4.2 *The affect of dust storm on air pollution index (API)*

For the purposes of further clarifying the affect of this dust storm on atmosphere aerosols and environmental air quality, we examined the API variation trends for 15–22 April at Beijing and Tianjin according to the released data from a Chinese Environmental Monitoring Station (Fig. 5). It can be seen from Fig. 5 that the API was 88 on 15 April at Beijing, while the average value was 148 for 16–21 April, and it declined to 58 again on 22 April, which indicated that the API was 1.68 and 2.25 times during dust weather than before and after dust weather. Meanwhile, the API was 73, 106, and 56 for 15, 16–21, and 22 April at Tianjin, respectively, and this indicated that the API in the dust storm period was 1.45 and 1.89 times than before and after this sandstorm. As a summary, this dust storm had a certain impact on Beijing and Tianjin air quality according to the above analysis, and dust storm weather can aggravate atmospheric pollution to an extent, an effect which cannot be ignored, especially in spring.

5. Simulation analysis and verification

5.1 *Simulation of dust storm process*

Figure 6 shows an average surface dust emission rate distribution for the dust storm of 15–22 April 2005. We can see that the dust source of this dust storm is mainly in western Inner Mongolia, and the dust emissions in northern Shaanxi and some areas of Xinjiang municipality and Mongolia are also visible. The difference of the surface dust emission rate in different regions is obvious, the maximum value is more than 300 μg m^{-2} s^{-1}.

Figure 7 displays the variations of dust AOD for 15–22 April simulated by RegCM3, and the moviement and change of high-value areas represent the trajectory and transport of dust particles. According to the simulation results, on 16 April this dust storm took shape in central and western Inner Mongolia, Gansu, Ningxia, and other northwestern regions and began to transport dust toward North China. On 17 April, high burdens of dust aerosol occurred in North China, and this dust continued to move in the southeasterward direction. We combined the simulation results with the Micaps weather situation (Fig. 2), and it can be seen that one cold front which originated in Mongolia and northwestern China further complemented and strengthened this sandstorm activity in degree and by extension during 18–19 April. This dust storm changed the atmospheric aerosol composition and environmental quality evidently in Northwest, North, Northeast, East, and the Central China according to the (section 4) analyses in this paper. Furthermore, high-burden areas of dust AOD migrated toward the southeast gradually, and the effect of dust storm weather in northern China basically ended after 21 April.

Figure 8 shows the dust aerosol average column burden for 15–22 April simulated by the model. We can see that the largest column burden is in northern Inner Mongolia, which exceeds 3 g m^{-2}. There is also another high column burden center distributed in northern Shaanxi and over the boundary of Inner Mongolia and Mongolia. In addition, the dust column burden of dust storm affected regions, especially in North China, including Shanxi, Henan, Hebei, Beijing, and parts of Shandong, Jiangsu, and Anhui, is about 0.3–0.9 g m^{-2}, which is greater than in North-

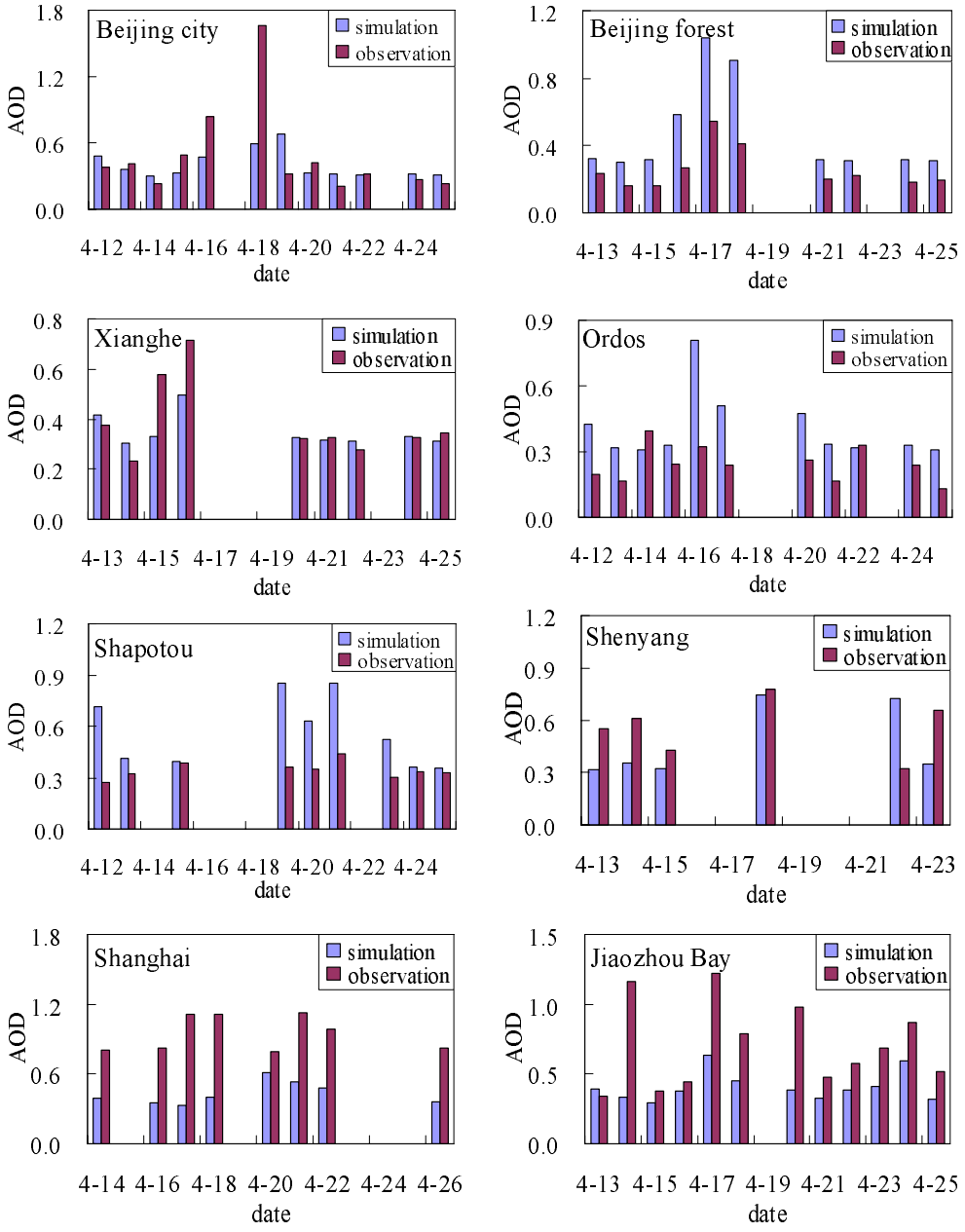

Fig. 9. The AOD simulation and observational comparison at 8 ground-based observational sites. Blue columns represent the simulation, and red columns represent observations.

east and South China.

5.2 *Analysis of simulation results*

In order to better compare the model simulation with ground-based observations, in addition to taking into account the sandstorm genesis, diffusion, variation, and sedimentation mechanisms for four different dust aerosol particles sizes, as well the increase of other aerosol types was also considered, including human and biological sulphur dioxide emissions (Emission Database for Global Atmospheric Research, EDGAR), human black carbon and organic carbon emissions (EDGAR), and biological black carbon and organic carbon emissions (LIOUSSE). Since the ground-based observational aerosol optical depth includes all aerosol effects (Table 1), it must have some dissimilarities between the simulation and observations.

RegCM3 can essentially simulate the AOD trends during this dust storm according to the comparison between observations and simulation (Fig. 9). The simulation for the Beijing city, Beijing forest, and Xianghe was much better and demonstrated the AOD

changes fairly well except for the simulation value at Beijing city which conspicuously lower on 18 April. As a whole, the simulation results were a bit higher at the Ordos and Shapotou sites, which may be since these two sites are located in dust-sand source regions and this model was quite sensitive to dust AOD variations in these areas. On the contrary, the AOD simulation results were obviously lower than observational data at the coastal Shanghai and Jiaozhou Bay sites, this may be due to fact that the observational AOD included various kinds of aerosol, especially sea salt particles, but the simulated AOD only included dust, sulfate, black carbon, and organic carbon, which caused the observational AOD to be larger than simulation to a certain extent.

6. Summary and conclusion

On the basis of the analysis of ground-based observational AOD and α in CSHNET and the API in Beijing and Tianjin during this dust storm period, this paper has fully discussed the effect of a dust storm on aerosol optical properties in China's central and northern regions, and employed the RegCM3 to simulate and verify the AOD variation trends. This serves a significant reference for the future improvement of model simulation ability. Its preliminary conclusions are as follows:

(1) According to the comparison and analysis of observational results, the AOD and API increased significantly while α had a decline during the dust storm period. AOD indicated a notable "Valley– Peak–Valley" pattern and α demonstrated a contrary "Peak–Valley–Peak" pattern in the stages of pre-dust storm, dust storm, and post-dust storm.

(2) The dust storm had an obvious effect on AOD, α, and API. When the dust storm occurred, AOD increased by 86%, 84%, 13%, 27%, 47%, 23%, and 24% at the Beijing city, Beijing forest, Xianghe, Shapotou, Shenyang, Shanghai, and Jiaozhou Bay, respectively, while the corresponding α decreases were 21%, 39%, 19%, 77%, 50%, 12%, and 21% at the Beijing city, Beijing forest, Xianghe, Ordos, Shapotou, Shanghai and Jizozhou Bay sites, respectively. The API for Beijing was 1.68 and 2.25 times during the dust weather than before and after the dust weather, and it was 1.45 and 1.89 times elevated in Tianjin compared to before and after the storm.

(3) RegCM3 can simulate the dust storm occurrence and path accurately and also can basically simulate the AOD trends compared with ground-based observations, and the largest dust aerosol column burden of this dust storm was in northern Inner Mongolia. The AOD simulation results for North China stations (Beijing city, Beijing forest, and Xianghe sites) were he best, and the simulation for dust-source stations (Ordos and Shapotou sites) was on the high side, while it was on the low side for coastal stations (Shanghai and Jiaozhou Bay sites).

Acknowledgements. This work was partly supported by the National Basic Research Program (No. 2007CB407303), National Natural Science Foundation of China (No. 40675073), and the 863 Program (No. 2006AA06A303). The authors are grateful to NASA/GSFC and the Chinese Ecosystem Research Network (CERN) stations managed by the Chinese Academy of Sciences for their contribution to this research.

REFERENCES

Acharya, Y. B., 2005: Spectral and emission characteristics of LED and its application to LED-based sunphotometry. *Optics and Laser Technology*, **37**, 547–550.

Brooks, D. R., and F. M. III. Mims, 2001: Development of an inexpensive handheld LED-based Sun photometer for the GLOBE program. *J. Geophys. Res.*, **106**, 4733–4740.

Chen, G. S., X. D. Liu, and B. D. Chen, 2006: Numerical simulations of spatial and temporal characteristics of airborne dust over Asia during springs of 2000 to 2002. *Environmental Science*, **27**, 1–8. (in Chinese)

Draxler, R. R., and G. D. Rolph, 2003: HYSPLIT (HYbrid Single-Particle Lagrangian Integrated Trajectory) Model. NOAA Air Resources Laboratory, Silver Spring, MD, 242pp. [Available at http://www.arl.noaa.gov/ready/hysplit4.html]

Du, W. P., J. Y. Xin, M. X. Wang, Q. X. Gao, Z. Q. Li, and Y. S. Wang, 2008: Photometric measurements of spring aerosol optical properties in dust and non-dust periods in China. *Atmos. Environ.*, **42**, doi: 10.1016/j.atmosenv.2008.06.043.

Elguindi, N., X. Q. Bi, F. Giorgi, B. Nagarajan, J. Pal, F. Solmon, S. Rauscher, and A. Zakey, 2007: RegCM Version 3.1 User's Guide, International Centre for Theoretical Physics, 58pp.

Formenti, P., W. Elbert, W. Maenhaut, J. M. Haywood, and M. O. Andreae, 2003: Chemical composition of mineral dust aerosol during the Saharan Dust Experiment (SHADE) airborne campaign in the Cape Verde region, September 2000. *J. Geophys. Res.*, **108**(D18), 8576, doi: 10.1029/2002JD002648.

Gao, X. J., Y. Luo, W. T. Lin, Z. C. Zhao, and F. Giorgi, 2003: Simulation of effect of land use change on climate in China by a regional climate model. *Adv. Atmos. Sci.*, **20**(4), 583–592.

Giorgi, F., 1986: A particle dry deposition parameterization scheme for use in tracer transport models. *J. Geophys. Res.*, **91**, 9794–9806.

Giorgi, F., 1989: Two-dimensional simulations of possi-

ble mesoscale effects of nuclear war fires. 1: Model description. *J. Geophys. Res.*, **94**, 1127–1144.

Giorgi, F., and W. L. Chameides, 1986: Rainout lifetimes of highly soluble aerosols and gasses as inferred from simulations with a general circulation model. *J. Geophys. Res.*, **91**, 14367–14376.

Gong, S. L., X. Y. Zhang, and T. L. Zhao, 2003: Characterization of soil dust aerosols in China and its transport and distribution during 2001 ACE-Asia: 2. Model simulation and validation. *J. Geophys. Res.*, **108**(D9), 4262, doi: 10.1029/2002JD002633.

Grell, G., 1993: Prognostic evaluation of assumptions used by cumulus Parameterizations. *Mon. Wea. Rev.*, **121,** 764–787.

Han, Z., H. Ueda, K. Matsuda, R. Zhang, K. Arao, Y. Kanai, and H. Hasome, 2004: Model study on particle size segregation and deposition during Asian dust events in March 2002. *J. Geophys. Res.*, **109**, D19205, doi: 10.1029/2004JD004920.

Hao, W. M., D. E. Ward, R. A. Susott, R. E. Babbitt, B. L. Nordgren, Y. J. Kaufman, B. N. Holben, and D. M. Giles, 2005: Comparison of aerosol optical thickness measurements by MODIS, AERONET sun photometers, and Forest Service handheld sun photometers in southern Africa during the SAFARI 2000 campaign. *International Journal of Remote Sensing*, **26**, 4169–4183.

Haywood, J., and Coauthors, 2003: Radiative properties and direct radiative effect of Saharan dust measured by the C-130 aircraft during SHADE: 1. Solar spectrum. *J. Geophys. Res.*, **108**(D18), 8577, doi: 10.1029/2002JD002687.

Holben, B. N., and Coauthors, 2001: An emerging ground-based aerosol climatology: Aerosol Optical Depth from AERONET. *J. Geophys. Res.*, **106**, 12067–12097.

Holtslag, A., B. De, and H. L. Pal, 1990: A high resolution airmass transformation model for short-range weather forecasting. *Mon. Wea. Rev.*, **118**, 1561–1575.

Kim, D. H., B. J. Sohn, T. Nakajima, T. Takamura, B. C. Choi, and S. C. Yoon, 2004: Aerosol optical properties over East Asia determined from ground-based sky radiation measurements. *J. Geophys. Res.*, **109**, D02209, doi: 10.1029/2003JD003387.

Kim, J., and Coauthors, 2006: Chemical apportionment of shortwave direct aerosol radiative forcing at the Gosan super-site, Korea during ACE-Asia. *Atmos. Environ.*, **40**, 6718–6729.

Kolev, N., I. Grigorov, I. Kolev, P. C. S. Devara, P. E. Raj, and K. K. Dani, 2007: Lidar and Sun photometer observations of atmospheric boundary-layer characteristics over an urban area in mountain valley. *Bound. Layer Meteor.*, **124**, 99–115.

Li, X., X. Q. Hu, C. X. Cui, and J. Li, 2005: Research on dust aerosol optical properties in South Tarim basin and classification of different dusty weather in China. *Journal of Desert Research*, **25**, 488–495. (in Chinese)

Liu, J. J., Y. F. Zheng, Z. Q. Li, and R. J. Wu, 2008: Ground-based remote sensing of aerosol optical properties in one city in Northwest China. *Atmospheric Research*, **89**, doi: 10.1016/j.atmosres.2008.01.010.

Mao, J. T., J. H. Zhang, and M. H. Wang, 2002: Summary comment on research of atmospheric aerosol in China. *Acta Meteorologica Sinica*, **60**, 625–634. (in Chinese)

Qian, J. H, F. Giorgi, and M. S. Fox-Rabinovitz, 1999: Regional stretched grid generation and its application to the NCAR RegCM. *J. Geophys. Res.*, **104** (D6), 6501–6513.

Qiu, J. H, H. B. Chen, P. C. Wang, Y. Liu, and X. A. Xia, 2007: Recent progress in atmospheric observation research in China. *Adv. Atmos. Sci.*, **24**, 940–953, doi: 10.1007/s00376-007-0940-x

Ogunjobi, K. O., Z. He, and C. Simmer, 2007: Spectral aerosol optical properties from AERONET Sunphotometric measurements over West Africa. *Atmospheric Research*, **88**, 89–107.

Rolph, G. D., 2003: Real-time Environmental Applications and Display sYstem (READY). NOAA Air Resources Laboratory, Silver Spring, MD, 25pp. [Available at http://www.arl.noaa.gov/ready/hysplit4.html].

Seinfeld, J. H., G. R. Carmichael, and R. Arimoto, 2004: ACE-ASIA: regional climatic and atmospheric chemical effects of Asian dust and pollution. *Bull. Amer. Meteor. Soc.*, **85**, 367–380.

Shao, L. Y., W. J. Li, S. S. Yang, Z. B. Shi, and S. L. Lü, 2007: Mineralogical characteristics of airborne particles collected in Beijing during a severe Asian dust storm period in spring 2002. *Science in China* (*D*), **50**, 953–959.

Shi, W. L., and H. J. Wang, 2003: The regional climate effects of replacing farmland and re-greening the desertification lands with forest or grass in west China. *Adv. Atmos. Sci.*, **20**, 45–54.

Solmon, F., F. Giorgi, and C. Liousse, 2006: Aerosol modeling for regional climate studies: Application to anthropogenic particles and evaluation over a European/African domain. *Tellus*, **58B**, 51–72.

Song, L. C., Y. X. Han, Q. Zhang, X. X. Xi, and Y. H. Ye, 2004: Monthly temporal–spatial distribution of sandstorms in China as well as the origin if Kosa in Japan and Korea. *Chinese J. Atmos. Sci.*, **28**, 820–828. (in Chinese)

Tegen, I., and I. Fung, 1994: Modeling of mineral dust in the Atmosphere: Sources transport and optical thickness. *J. Geophys. Res.*, **99**, 22897–22914.

Tian, H., J. Z. Ma, W. L. Li, and H. L. Liu, 2005: Simulation of forcing of sulfate aerosol on direct radiation and its climate effect over middle and eastern China. *Journal of Applied Meteorological Science*, **16**, 322–333. (in Chinese)

Wang, H., G. Y. Shi, B. Wang, W. Li, S. Y. Li, S. L. Gong, and T. L. Zhao, 2007a: The impact of dust aerosol from deserts of China on the radiative heating rate over sources and the North Pacific region.

Chinese J. Atmos. Sci., **31**, 515–526. (in Chinese)

Wang, Y., G. S. Zhuang, A. H. Tang, W. J. Zhang, Y. L. Sun, Z. F. Wang, and Z. S. An, 2007b: The evolution of chemical components of aerosols at five monitoring sites of China during dust storms. *Atmos. Environ.*, **41**, 1091–1106.

Wang, Y., and Coauthors, 2008: Seasonal variations in aerosol optical properties over China. *Atmospheric Chemistry and Physics Discuss*ions, **8**, 8431–8453.

Won, J. G., S. C. Yoon, S. W. Kim, A. Jefferson, E. G. Dutton, and B. N. Holben, 2004: Estimation of direct radiative forcing of Asian dust aerosols with Sun/sky radiometer and lidar measurements at Gosan, Korea. *J. Meteor. Soc. Japan*, **82**, 115–130.

Wu, J., Y. Xu, C. Fu, R. Zhang, M. Dai, and Y. Zhu, 2006: Comparison of simulating mineral dust aerosol in East Asia by two emission schemes. *China Particuology*, **4**(6), 293–299.

Xin, J. Y., and Coauthors, 2007: Aerosol optical depth (AOD) and Angstrom exponent of aerosols observed by the Chinese Sun Hazemeter Network from August 2004 to September 2005. *J. Geophys. Res.*, **112**, doi: 10.1029/2006JD007075.

Xin, J. Y., Y. S. Wang, Z. Q. Li, P. C. Wang, S. G. Wang, T. X. Wen, and Y. Sun, 2006: Introduction and calibration of the Chinese Sun Hazemeter Network. *Environmental science*, **27**, 1697–1702. (in Chinese)

Xuan, J., G. L. Liu, and K. Du, 2000: Dust emission inventory in Northern China. *Atmos. Environ.,* **34**, 4565–4570.

Zakey, A. S., F. Solmon, and F. Giorgi, 2006: Development and testing of a desert dust module in a regional climate model. *Atmospheric Chemistry and Physics Discuss*ions, **6**, 1749–1792.

Zender, C. S., H. Bian, and D. Newman, 2003: Mineral dust entrainment and deposition (DEAD) model: Description and 1990s dust climatology. *J. Geophys. Res.*, **108**, 4416, doi: 10.1029/2002JD002775.

Zeng, X., M. Zhao, and R. E. Dickinson, 1998: Intercom-Parison of bulk aerodynamic algoriths for the computation of sea surface fluxes using TOGA COARE and TAO data. *J. Climate*, **11**, 2628–2644.

Zhang, L., S. Gong, J. Padro, and L. Barrie, 2001: A size-segregated particle dry deposition scheme for an atmospheric aerosol module. *Atmos. Environ.*, **35**, 549–560.

Zhang, R. J., M. X. Wang, L. F. Sheng, Y. Kanai, and A. Ohta, 2004: Seasonal Characterization of dust days, mass concentration and dry deposition of atmospheric aerosol over Qingdao, China. *China Particuology*, **2**(5), 196–199.

Zhang, X. Y., 2001: Source distributions, emission, transportation, deposition of Asia dust and loess accumulation. *Quaternary Science*, **21**, 29–40. (in Chinese)

Zhang, X. Y., G. Y. Zhang, G. H. Zhu, D. E. Zhang, Z. S. An, T. Chen, and X. P. Huang, 1996: Elemental tracers for Chinese source dust. *Science in China* (*D*), **26**, 512–521.

Zhang, X. Y., R. Arimoto, and Z. S. An, 1997: Dust emission from Chinese desert sources linked to variations in atmospheric circulation. *J. Geophys. Res.*, **102**(D23), 28041–28047.

Zhou, X. J., X. D. Xu, P. Yan, Y. H. Weng, and J. L. Wang, 2002: Dynamic characteristics of spring sandstorms in 2000. *Science in China* (*Series D*), **45**, 921–930.

Zhang, X. Y., S. L. Gong, T. L. Zhao, R. Arimoto, Y. Q. Wang, and Z. J. Zhou, 2003a: Sources of Asian dust and role of climate change versus desertification in Asian dust emission. *J. Geophys. Res.*, **30**(24), 2272, doi: 10.1029/2003GL018206.

Zhang, X. Y., and Coauthors, 2003b: Characterization of soil dust aerosol in China and its transport/distribution during 2001 ACE-Asia: 1. Network observations. *J. Geophys. Res.*, **108**, 4261, doi: 10.1029/2002JD002632.